Journal of Power Sources 243 (2013) 773–778

Contents lists available at SciVerse ScienceDirect

Journal of Power Sources

journal homepage: www.elsevier.com/locate/jpowsour

Water uptake, ionic conductivity and swelling properties of anion-exchange membrane

Qiongjuan Duan [a,b], Shanhai Ge [a], Chao-Yang Wang [a,*]

[a] Electrochemical Engine Center (ECEC), and Department of Mechanical and Nuclear Engineering, The Pennsylvania State University, University Park, PA 16802, USA

[b] State Key Laboratory for Modification of Chemical Fibers and Polymer Materials, College of Material Science and Engineering, Donghua University, Shanghai 201620, PR China

HIGHLIGHTS

- The swelling properties of the A201 membrane are investigated at different temperatures.
- Water sorption of the A201 membrane occurs with negative excess volume of mixing.
- Percolative nature of the ion transport has been identified in the A201 membrane.

ARTICLE INFO

Article history:
Received 21 February 2013
Received in revised form
14 June 2013
Accepted 17 June 2013
Available online 25 June 2013

Keywords:
Anion-exchange membrane
Water uptake
Conductivity
Dimensional change
Excess volume of mixing

ABSTRACT

Water uptake, ionic conductivity and dimensional change of the anion-exchange membrane made by Tokuyama Corporation (A201 membrane) are investigated at different temperatures and water activities. Specifically, the amount of water taken up by membranes exposed to water vapor and membranes soaked in liquid water is determined. The water uptake of the A201 membrane increases with water content as well as temperature. In addition, water sorption data shows Schroeder's paradox for the AEMs investigated. The swelling properties of the A201 membrane exhibit improved dimensional stability compared with Nafion membrane. Water sorption of the A201 membrane occurs with a substantial negative excess volume of mixing. The threshold value of hydrophilic fraction in the A201 membrane for ionic conductivity is around 0.34, above which, the conductivity begins to rise quickly. This indicates that a change in the connectivity of the hydrophilic domains occurs when hydrophilic fraction approaches 0.34.

1. Introduction

With the advantages of using non-precious electrocatalysts and reduced corrosion problems, anion-exchange membrane fuel cells (AEMFCs) have become a very promising energy conversion technology, and are expected to be an alternative to proton exchange membrane fuel cells (PEMFCs). The chemical reactions in hydrogen fueled traditional AEMFCs are presented below:

$$\text{Anode}: \ 2H_2 + 4OH^- \rightarrow 4H_2O + 4e^-; \ E_{\text{anode}} = -0.828\text{V} \quad (1)$$

$$\text{Cathode}: \ O_2 + 2H_2O + 4e^- \rightarrow 4OH^-; \ E_{\text{cathode}} = 0.401\text{V} \quad (2)$$

$$\text{Overall}: \ 2H_2 + O_2 \rightarrow 2H_2O; \ E_{\text{cell}} = 1.229\text{V} \quad (3)$$

Oxygen is reduced at the cathode to produce OH^-, which transports through the anion-exchange membrane (AEM) to the anode side and combines with the hydrogen to generate water [1].

At the heart of the AEMFC, the AEM is one of the most significant components contributing to cell performance. In the last few years, significant effort has been devoted to development and synthesis of AEMs [2–5]. However, a commercial AEM with performance similar to PEMFC with Nafion membrane is still unavailable. Since the emergence of a commercial AEM tailored for AEMFC by Tokuyama Corporation, the performance and durability of the AEMFC achieved a substantial improvement. Nevertheless, it is still far below current PEMFC performance.

Similar to Nafion membrane, AEM can conduct ions only in the presence of water. In addition, water is one of the reactants in the oxygen reduction reaction. Therefore, humidified gases are fed into

* Corresponding author.
E-mail address: cxw31@psu.edu (C.-Y. Wang).

0378-7753/$ – see front matter © 2013 Elsevier B.V. All rights reserved.
http://dx.doi.org/10.1016/j.jpowsour.2013.06.095

the fuel cell under most operating conditions. Water content of the AEM and ionomer varies with current, which also affects the transport properties of the AEM. Decrease in water content leads to a reduction of conductivity of the AEM, which might cause ohmic loss.

Currently, the A201 membrane from Tokuyama is the most popular and commercially available AEM used in AEMFCs. It is 28 μm in thickness at dry state, consists of hydrocarbon backbone and quaternary ammonium functional groups terminated side chains. In the last few years, many in-situ experiments have been completed by researchers to investigate performance, durability, CO_2 tolerance and electro-osmotic drag coefficient of the A201 membrane [6–11]. Ex-situ testing for sorption and diffusion of water in the A201 membrane were also performed. Li et al. [12] measured water uptake of A201 membrane under different relative humidities at 30, 40 and 60 °C, and found that Schroeder's paradox existed in the AEM. They reported that the water diffusion coefficient in the membrane is in the order of 10^{-10} m^2 s^{-1}, which is close to Nafion membrane. They also reported that the water transfer coefficient is in the range of 10^{-6}–10^{-5} m^{-1}. However, the swelling properties of the A201 membrane have not being studied in recent publications. As water is absorbed in the membrane, the hydrophilic domains swell with increasing hydration. How does the swelling of the membrane affect the ion transport through the A201 membrane? Since the ion transport is basically related to the network structure of functional groups associated with water, the answer to this question requires more detailed research about the conductivity and microstructure of the AEM as a function of water content.

To better understand the transport mechanisms and swelling properties of the AEM, we did ex-situ membrane tests with well established techniques and equipment for studying various properties [13]. The objective of this work is to investigate the membrane conductivity and the dimensional change as functions of temperature and water content of the membrane.

2. Experimental

2.1. Materials

AEM, A201 membrane with ion exchange capacity (IEC) of 1.7 mmol g^{-1} was provided by Tokuyama Corporation, Japan. The membrane characterized in this paper was not pretreated. Deionized water was used in all the experiments.

2.2. Water uptake & conductivity

Water uptake and ionic conductivity were measured in an isometric system at different temperatures and water vapor pressures [14].

A membrane sample was placed in a chamber with fixed volume, which was evacuated at a test temperature below 1 Pa to remove any residual water in the membrane as well as in the chamber. A small amount of water (5–40 μL) injected into the chamber was observed to evaporate very quickly. Ideal gas law associated with the vaporization of the injected water was used to determine the expected pressure (theoretically), p_{exp}.

$$p_{exp} = \frac{m_w RT}{M_w V} \tag{4}$$

where V is the volume of chamber, m_w the mass of water injected, R universal gas constant, T temperature, and M_w the molecular weight of water. After the membrane is equilibrated with water vapor, the actual pressure, p_{act} can be determined by the pressure transducer in the chamber. The difference between p_{exp} and p_{act} is attributed to the water absorbed by the AEM. The mole of water absorbed by the membrane (n_w) is calculated by the following equation:

$$n_w = \frac{V\left(p_{exp} - p_{act}\right)}{RT} \tag{5}$$

Membrane water content is determined by the activity of water vapor in the chamber since equilibrium is assumed. The activity in the vapor phase (a_w) is

$$a_w = \frac{p_{act}}{p_{sat}} \tag{6}$$

where p_{sat} is the saturation pressure of water. The water content of the membrane (λ) is calculated by dividing n_w with IEC and the mass of the membrane (m_m):

$$\lambda = \frac{n_w}{IEC \cdot m_m} \tag{7}$$

Water uptake of the AEM in equilibrium with liquid water was measured by weighing the membranes before and after soaking in the liquid water for 24 h.

Within the chamber, the ionic conductivity of the membrane was measured by an AC impedance technique in the surface direction (in-plane). The membrane was cut into 2 cm wide × 4 cm long pieces. Fig. 1 shows the schematic of test equipment for membrane resistance measurement. Each sample was clamped between a set of graphite electrodes spaced 0.17 cm apart. Conductivity of the membrane was calculated using the following equation.

$$\sigma = \frac{L}{R_m A} \tag{8}$$

where σ is conductivity (S cm^{-1}), L the distance between two electrodes (cm), A cross area of the membrane (cm^2), and R_m the measured resistance of the membrane (Ω).

2.3. Dimensional change

The dimensional change of the AEM was also measured as functions of temperature and water activity using a custom built creep instrument within an environmental chamber [15]. Samples were cut into 3 cm long, 1 cm wide pieces and clamped in the jaw of the creep instrument and dried in N_2 at 80 °C for 2 h before testing. A small stress (0.05–0.1 MPa) was applied on the sample to pull it straight such that no creep would occur in this situation. After drying the sample, the temperature in the chamber was adjusted to the desired test temperature. Water vapor was introduced by feeding the chamber with humidified N_2. The length of the sample was monitored in real time as the water activity in the chamber was held stable. The equilibrium dimensional change was recorded when the rate of length change was smaller than 0.1% h^{-1}. The

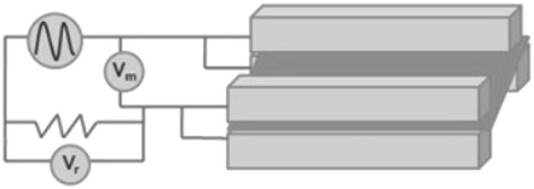

Fig. 1. Schematic of the test equipment for membrane resistance measurement.

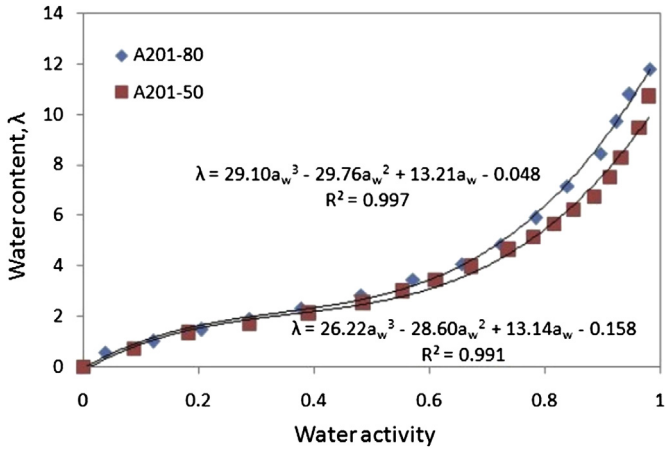

Fig. 2. Isotherms of water content of the AEMs as a function of water activity at different temperatures.

equilibrium dimensional change was measured at 50 and 80 °C with water activity rising from 0 to 0.95 at intervals of around 0.05.

3. Results and discussion

3.1. Water uptake

As shown in Fig. 2, sigmoid isotherm curves as a function of water activity were obtained for A201 membrane. Investigating the water content of the membrane response with increasing water activity gives an idea how water activity is affecting water uptake of the membrane. The plots show a rapid rise of water content at low water activity, a slower rise to plateau at a_w range of 0.1–0.5 and the majority of water content occurring at $a_w > 0.5$. Comparing with water content at 50 and 80 °C, it is clear that the curves are very similar, but at higher water activity ($a_w > 0.4$), water content is larger at 80 °C.

The water content of A201 membrane in equilibrium with saturated water vapor ($a_w = 1$), are 11.5 and 10.0 at 80 and 50 °C, respectively. This water content is very close to those of Nafion membrane (14.0 at 30 °C, 9.7 at 80 °C) [16–18]. Because the IEC of A201 membrane is 1.7 mmol g^{-1}, which is much higher than the Nafion membrane EW1100 series (0.91 mmol g^{-1}), the total water uptake of the AEM is higher than that of Nafion membrane.

For membrane in equilibrium with liquid water, the water uptake was measured by weighing the membranes before and after soaking them into the liquid water for 24 h. Fig. 3 shows water contents of A201 membrane equilibrated with liquid water. It is found that the water content increases gradually with temperature, which suggests a linear relationship. Comparing with the membrane water uptakes in water vapor, water uptake in liquid water is greater. The different water uptakes of the membrane in equilibrium with water vapor and liquid water indicate that Schroeder's paradox can be found in AEM.

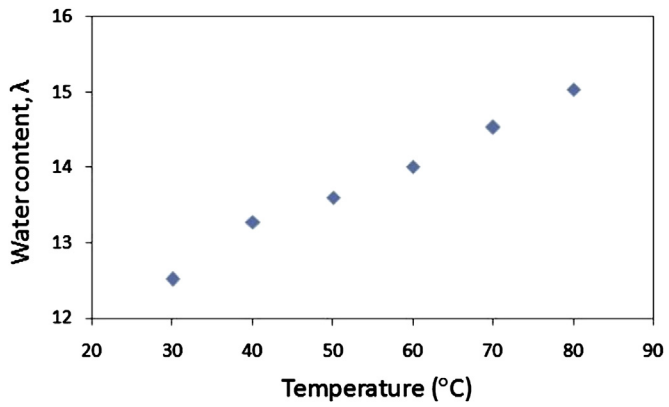

Fig. 3. Water contents of A201 membrane equilibrated with liquid water.

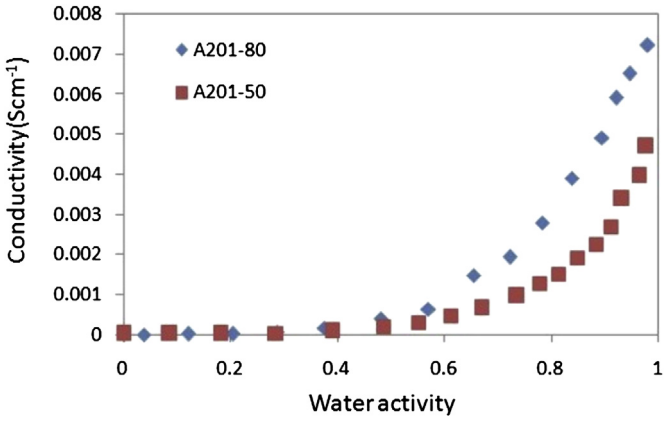

Fig. 4. Ionic conductivities of AEM at 50 and 80 °C as a function of water activity.

3.2. Conductivity

The AEM usually converts from OH^- form to HCO_3^- form after exposure in air because of the existence of CO_2. Since it is very difficult to measure the conductivity of the AEM in the pure OH^- form, the membranes studied in this experiment are all HCO_3^- form. No further treatment was undertaken for the membranes.

Fig. 4 shows the ionic conductivity of AEM at 50 and 80 °C as a function of water activity. At low water activity ($a_w < 0.5$), the conductivities of A201 membrane at different temperatures are nearly the same. The ionic conductivities are smaller than 0.2 mS cm^{-1}. At high water activity ($a_w > 0.5$), the conductivities at both temperatures increase exponentially. Fig. 4 also shows that the membrane conductivity at high water activity at 80 °C is much greater than that at 50 °C. Ion mobility for OH^- is about 4 times higher than HCO_3^- form [2]. For this reason, the ionic conductivity in our case is much lower than the data reported by Tokuyama Corporation (~0.04 S cm^{-1} at 23 °C and $a_w = 0.9$) [6].

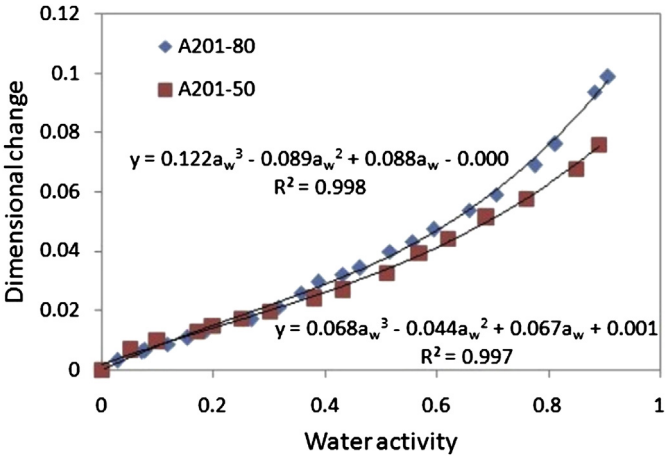

Fig. 5. Dimensional changes of A201 membrane with water vapor activity at different temperatures.

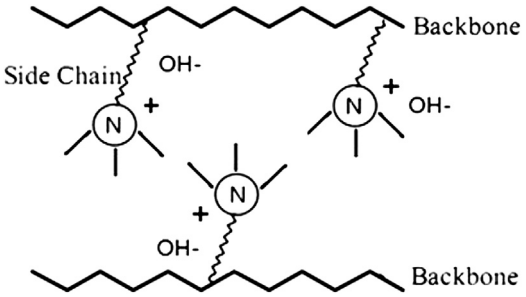

Fig. 6. Schematic of the AEM structure.

3.3. Dimensional change

The ability to swell is an important property of AEM. Understanding of swelling behavior might shed light on the understanding of ion transfer inside the membrane and microstructure of the membrane. Dimensional change of the membranes depends on water sorption and scales with water activity. Fig. 5 shows dimensional changes of A201 membrane with water vapor activity at different temperatures. Sigmoid isotherm curves as a function of water activity were also obtained for dimensional change of A201 membrane. Similar to the water uptake plots, the dimensional changes at low water activity are quite close. However, at higher water activity, swelling of the membrane at 80 °C is much larger than that at 50 °C.

As mentioned in the Introduction, the AEM in our study is composed of hydrocarbon polymer backbone and side chain end-functionized with quaternary ammonium groups. The structure of the membrane is illustrated in Fig. 6. The difference in the polarity of the side chain and the hydrocarbon backbone leads to the segregation of the membrane into hydrophilic and hydrophobic regions.

Water interacts with the quaternary ammonium group, leading to the swelling of the hydrophilic domains surrounded by the hydrophobic hydrocarbon polymer backbone. It is clear that when water activity is around 1, the dimensional changes of A201 membrane are 9% and 12% at 50 and 80 °C respectively, as shown in Fig. 5. Like almost all polymers, AEMs become more flexible at higher temperature. Additionally, comparing with the swelling properties of Nafion membrane [19], the AEMs that we have tested exhibit better dimensional stability.

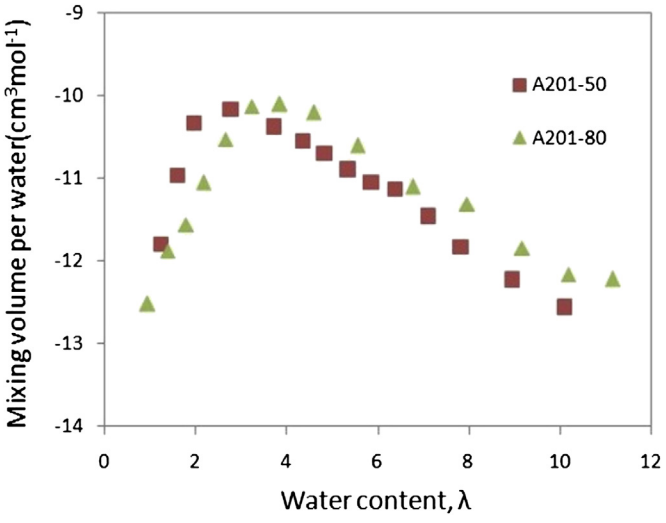

Fig. 7. Excess volume of mixing of water and AEMs per water molecule absorbed as a function of water content at different temperatures.

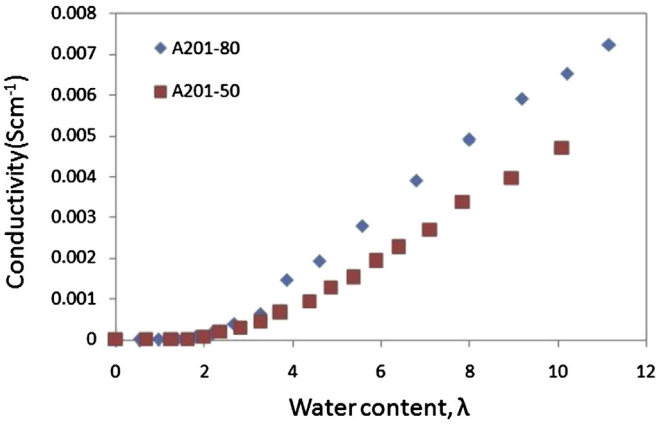

Fig. 8. Ionic conductivities of AEM at 50 and 80 °C as a function of water content.

3.4. Excess volume of mixing (combination of water sorption and swelling data)

The volume expansion (cm^3) of the membrane minus the volume of absorbed water is determined as excess volume of mixing.

$$V_{evm} = V_{expansion} - V_w \tag{9}$$

where V_{evm} is excess volume of mixing (cm^3), $V_{expansion}$ expansion volume (cm^3) of the membrane, and V_w absorbed water volume (cm^3). The excess volume of mixing was normalized according to the absorbed mole of water (n_w) and plotted as a function of water content in Fig. 7.

$$\Delta V_m = \frac{V_{expansion} - V_w}{n_w} \tag{10}$$

It is found in our experiment that the AEM has a substantial negative excess volume of mixing per molar absorbed water. As a mole of water has a volume of 18 cm^3, the data in Fig. 7 suggests the AEM has void spaces such as microcavities and micropores which permits the membrane to absorb water with little bulk volume change, which is 7 ± 1 cm^3 per mole absorbed water molecule. As

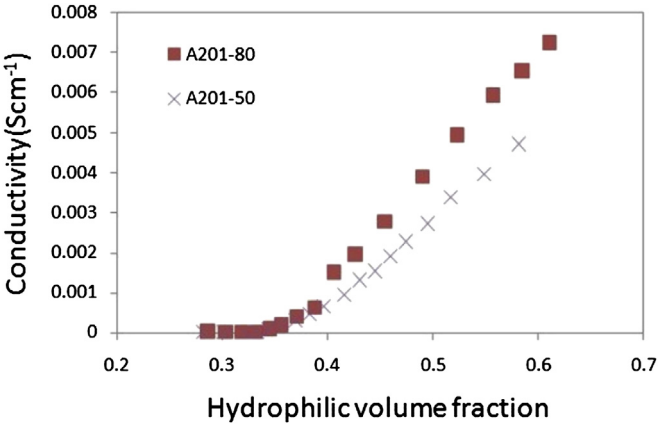

Fig. 9. Ionic conductivities of AEM at 50 and 80 °C as a function of hydrophilic volume fraction.

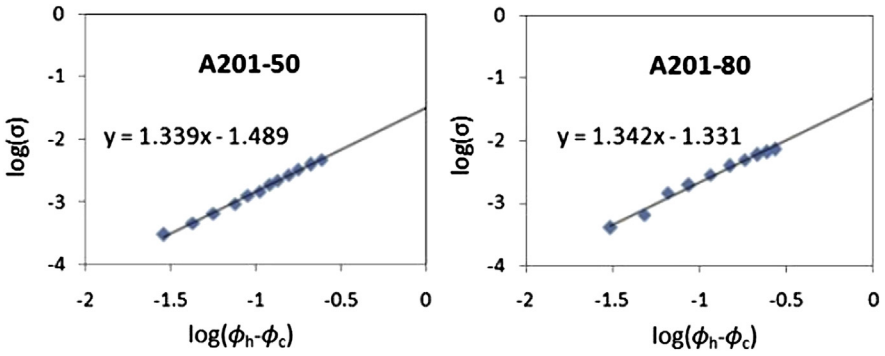

Fig. 10. Log–log plots of σ vs $(\phi_h - \phi_c)$ for AEM at different temperatures.

water is absorbed by the membrane, balance between the energy of hydration of the functional groups and the energy to swell the surrounding hydrocarbon matrix has to be readapted, leading to the expansion of the membrane. At low water activity, the absorbed water strongly interacts with functional groups and begins to fill into the membrane. When $\lambda < 3$, the ΔV_m slowly increase with λ to a maximum of about -10 cm^3 mol^{-1} at $\lambda = 3$. When $\lambda > 3$, ΔV_m slowly decreased toward -12 cm^3 mol^{-1}. We suggest a secondary hydration shell begins to form at $\lambda = 3$, in this process, water is weakly bonded to the functional groups and becomes more easily squeezed into micropores of the membrane.

Ionic conductivities of the AEMs at 50 and 80 °C as a function of water content are plotted in Fig. 8. It is found that when water content is higher than 3, the conductivity rises very quickly, which suggests that a change in the connectivity of the hydrophilic domains occurs at $\lambda \approx 3$. We suggest there is a secondary hydration shell being formed when $\lambda > 3$. It fills in the micropores of the membrane and creates more paths for ion transport.

Ion transport is mainly influenced by the microstructure of the membrane. As the hydrophilic fraction in the membrane increases, the isolated hydrophilic domain will expand and become interconnected with hydration. Eventually, a critical hydrophilic volume fraction, ϕ_c is reached and the channels for ion transport become possible. The greater the dimension of the functional group and absorbed water molecules, the higher the ionic conductivity.

Percolation theory applied to Nafion membrane decades ago [20] suggests that water sorption swells the hydrophilic region and build up channels for proton transport through the membrane. Herein we apply this theory to AEM as well.

We hypothesize a threshold value for the amount of hydrophilic region, below which ion transport is very difficult and slow due to lack of ion conducting pathway. When the hydrophilic region is greater than the threshold value, the conductivity of the membrane would increase and begin to show very strong dependence on water content.

The dimensional change data with water sorption in Fig. 5 are combined with the conductivity data to identify the percolation threshold. Eq. (11) is used to calculate the hydrophilic volume fraction in the AEM. This is given by the sum of the volume fraction of the functional group and absorbed water in swelled membrane:

$$\phi_h = \frac{V_w + \frac{M_m \cdot V_f}{EW}}{V_s} \tag{11}$$

where ϕ_h is hydrophilic fraction in the membrane, V_w the volume of the absorbed water, V_f the molar volume of the functional group, which is the sum of molar volume of N $(CH_3)_3^+$ and HCO_3^-, M_m the mass of the tested membrane, and V_s the volume of the swollen membrane.

Fig. 9 is a plot of the conductivity as a function of the hydrophilic volume fraction. The percolation threshold for the ionic conductivity can be determined from the onset of rapid increase in the ionic conductivity. The critical hydrophilic volume fraction, ϕ_c is around 0.34 at both temperatures.

Above the threshold value, the conductivity should follow the power law:

$$\sigma = \sigma_0(\phi_h - \phi_c)^n \tag{12}$$

In our case, the ϕ_c is found to be 0.34. We plotted log (σ) vs log $(\phi_h - \phi_c)$ and found a linear relation, as shown in Fig. 10. The slopes of the lines were around 1.34, which means $n \approx 1.34$. σ_0 are 0.23 and 0.26 at 50 and 80 °C, respectively.

The exponent n is a constant and only depends on the spatial dimension. It is reported that for a three dimensional system, n falls in the range of 1.3–1.7 [21], which suggests that the hydrophilic region in the AEM fits into the three dimensional system. The threshold value depends on the dimension and dispersion of the hydrophilic domain. The percolation threshold $\phi_c = 0.34$ for AEM indicates that the functional groups in the membrane aggregate as cubic domains and randomly dispersed in the polymer matrix [22].

4. Conclusions

Water uptake isotherms have been measured at 50 and 80 °C for A201 membrane in equilibrium with water vapor. The water uptake of the AEM increases with water activity as well as with temperature. In addition, water sorption data shows Schroeder's paradox for the AEM investigated.

This work is the first systematic report of the dimensional change of A201 membrane as a function of water activity. Dimensional changes of A201 membrane at water activity of 1 are 9% and 12% at 50 and 80 °C, respectively. In addition, the AEMs that we have tested exhibit better dimensional stability than Nafion membrane. Ionic conductivity of the AEM begins to increase and shows very strong dependence on water content (λ) until $\lambda > 3$. In addition, the excess volume of mixing shows a maximum at $\lambda \approx 3$. This indicates that the first hydration shell of 3 water molecules is formed in the membrane, and the second hydration shell is formed when $\lambda > 3$. The percolation nature of ion transport has been identified in the AEM. The percolation threshold for A201 membrane is 0.34 of hydrophilic volume fraction, which suggests that AEM has cubic hydrophilic domains with random dispersion.

Acknowledgments

Partial support of this work by the Advanced Research Projects Agency – Energy (ARPA-E) under Award Number DE-AR0000121 is gratefully acknowledged. Prof. Jay Benziger at Princeton University and his group members are acknowledged for help and discussion, and Tokuyama Corporation for supplying membrane materials. Q. Duan is supported by a fellowship from the Chinese Scholarship Council.

References

[1] J.R. Varcoe, R.C.T. Slade, Fuel Cells 5 (2005) 187–200.
[2] J.L. Yan, M.A. Hickner, Macromolecules 43 (2010) 2349–2356.
[3] J.R. Varcoe, R.C.T. Slade, Electrochem. Commun. 8 (2006) 839–843.
[4] O.I. Deavin, S. Murphy, A.L. Ong, S.D. Poynton, R. Zeng, H. Herman, J.R. Varcoe, Energy Environ. Sci. 5 (2012) 8584–8589.
[5] X.M. Yan, G.H. He, S. Gu, X.M. Wu, L.G. Du, H.Y. Zhang, J. Membr. Sci. 375 (2011) 204–211.
[6] H. Yanagi, K. Fukuta, ECS Trans. 16 (2008) 257–262.
[7] L. An, T.S. Zhao, Y.S. Li, Q.X. Wu, Energy Environ. Sci. 5 (2012) 7536–7538.
[8] Y.J. Leng, G. Chen, A.J. Mendoza, T.B. Tighe, M.A. Hickner, C.Y. Wang, J. Am. Chem. Soc. 134 (2012) 9054–9057.
[9] Y.S. Li, T.S. Zhao, Int. J. Hydrogen Energy 36 (2011) 7707–7713.
[10] Z. Siroma, S. Watanabe, K. Yasuda, K. Fukuta, H. Yanagi, J. Electrochem. Soc. 158 (2011) B682–B689.
[11] X.H. Wang, J.P. McClure, P.S. Fedkiw, Electrochim. Acta 79 (2012) 126–132.
[12] Y.S. Li, T.S. Zhao, W.W. Yang, Int. J. Hydrogen Energy 35 (2010) 5656–5665.
[13] X.M. Wu, X.W. Wang, G.H. He, J. Benziger, J. Polym. Sci. Pol. Phys. 49 (2011) 1437–1445.
[14] C. Yang, S. Srinivasan, A.B. Bocarsly, S. Tulyani, J.B. Benziger, J. Membr. Sci. 237 (2004) 145–161.
[15] P.W. Majsztrik, A.B. Bocarsly, J.B. Benziger, Rev. Sci. Instrum. 78 (2007), 103904-1–103904-7.
[16] T.A. Zawodzinski, C. Derouin, S. Radzinski, R.J. Sherman, V.T. Smith, T.E. Springer, S. Gottesfeld, J. Electrochem. Soc. 140 (1993) 1041–1047.
[17] J.T. Hinatsu, M. Mizuhata, H. Takenaka, J. Electrochem. Soc. 141 (1994) 1493–1498.
[18] S.H. Ge, X.G. Li, B.L. Yi, I.M. Hsing, J. Electrochem. Soc. 152 (2005) A1149–A1157.
[19] Q. Zhao, P. Majsztrik, J. Benziger, J. Phys. Chem. B 115 (2011) 2717–2727.
[20] W.Y. Hsu, T.D. Gierke, J. Membr. Sci. 13 (1983) 307–326.
[21] W.Y. Hsu, J.R. Barkley, P. Meakin, Macromolecules 13 (1980) 198–200.
[22] M.H. Cohen, J. Jortner, I. Webman, Phys. Rev. B 17 (1978) 4555–4557.